A NEW SUBGRID-SCALE STRESS TRANSPORT MODEL AND ITS APPLICATION TO LES OF EVOLVING COMPLEX TURBULENT FLOWS

Bruno Chaouat
Department of Computational Fluid Dynamics, ONERA
BP 72 - 92322 Châtillon cedex, France
Bruno.Chaouat@onera.fr

Roland Schiestel
IRPHE CNRS/Universités d'Aix-Marseille I & II
Technopôle Château-Gombert, BP 146 - 13384 Marseille cedex 13, France
Roland.Schiestel@irphe.univ-mrs.fr

ABSTRACT

A new partialy integrated transport model (PITM) for subgrid-scale stresses and dissipation rate is proposed for Large eddy simulations using relatively coarse grids of unsteady flows which present non-equilibrium turbulence spectra. The use of transport equations for all the subgrid-scale stress components allows to take into account more precisely the turbulent processes of production, transfer, pressure redistribution effects and dissipation, and the concept of turbulent viscosity is no longer necessary. In this study, a formally consistent derivation of the model is obtained when the cutoff location is varied, which guaranties compatibility with the two extreme limits that are the full statistical Reynolds stress transport model and direct numerical simulation. So, this approach enables to bridge URANS and LES methods with "seamless coupling "(Hanjalic et al., 2004). The present model is first against on the well known fully developed turbulent channel flow. The applications to the channel flow with wall mass injection are successfully performed for two different channel heights. The flows are characterized by the development of natural unsteadiness with a transition process from laminar to turbulent regime or by an acoustic resonant regime subjected to the vortex shedding mechanism.

INTRODUCTION

Advanced statistical models based on the Reynolds Averaged Navier-Stokes Equations (RANS) such as the Reynolds Stress Models (RSM) (Launder 1989, Speziale et al. 1991) can be able to accurately predict complex flows for engineering applications, as for instance flows with strong effects of streamline curvature, system rotation or wall injection (Chaouat, 2001). However, these models based on one point closure are not well suited for unsteady flows subjected to medium range frequencies that can interact with the turbulence scales and they cannot provide information on turbulence structures, two-point correlation statistics or energy spectrum which can be useful for investigating the flow characteristics. Contrary to full statistical modeling, LES enables to mimic the mechanisms of turbulent interactions, and informations on velocity or pressure fluctuations and on two-point correlations are possible. New trends in LES of turbulence have been proposed in the past decade, such as for instance the dynamic model (Germano et al., 1992), the structure model (Lesieur and Metais, 1992). Deardorff (1973) has developed a model which lies on the transport equations of the subgrid scale turbulent stresses with an algebric relation for the length scale. Despite improvements in the more advanced approaches, several modeling problems remain. Among these problems, for instance, the filter width may no longer be a good estimate of the characteristic subgrid-scale turbulence length when the filter cutoff is located at a wave number below the inertial range in non-equilibrium flows. To overcome this problem, Schiestel and Dejoan (2005) have developed a new subgrid scale model based on two transport equations for the subgrid-scale energy and the dissipation rate ϵ equation. In that approach, the transport equation for the dissipation rate is used for calculating the length scale without referring directly to the mesh size. The aim of the present study is to propose a new LES approach involving all the stress transport equations of the subgrid-scale turbulence including also the dissipation rate equation (Chaouat and Schiestel, 2005). This modeling strategy is motivated by the idea that the recognized advantages of usual second order closures (RSM) are worth to be transposed to subgrid-scale modeling when the SGS part is not small compared to the resolved part. In particular, due to the presence of the subgrid-scale pressure-strain correlation term in the transport equations, this new model embodies interesting features allowing a more realistic description of the flow anisotropy than eddy viscosity models, and also a better account of history and nonlocal effects. The model formulation is built such that the new subgrid-scale model complies with the two extreme limits that are DNS and full statistical Reynolds stress model in a continuous way. This behavior allows the development of hybrid models that enables to bridge URANS and LES methods with "seamless coupling "(Hanjalic et al., 2004). Recently, this line of thought appeared to gain major interest in turbulence modeling (Spalart, 2000). The main applications will be concerned with simulations of turbulent flows which undergo non-equilibrium changes such as produced by unsteadiness (forced or natural) in the mean or strong spatial variations on relatively coarse grids. In order to calibrate the present model, LES of fully developed turbulent channel flow is performed and the Reynolds stresses components are compared with available DNS data (Moser et al.,

1999). The application to the channel flow with wall injection is then considered for illustrating the potentials of the method. This case is of central interest for engineering applications in Solid Rocket Motors (SRM). The mass transfer resulting from the propellant combustion (represented by the mass injection at the wall) produces an internal flow field with different flow regimes, from laminar to turbulent, which affects the ballistics predictions of the rocket (Chaouat and Schiestel, 2002).

GOVERNING EQUATIONS

We consider the turbulent flow of a viscous fluid. As in the usual treatment of turbulence, the flow variable ξ is decomposed into a filtered part $\bar{\xi}$ including mean value and large-scale fluctuation and a subgrid-scale fluctuating part ξ' such that $\xi = \bar{\xi} + \xi'$. The quantity $\bar{\xi}$ is defined by the filter function G_Δ in physical space. The Reynolds statistical average of ξ is denoted by $< \xi >$ so that the large scale fluctuation is $\bar{\xi} - < \xi >$. In the present case, the Favre averaging is used for compressible flows. In that definition, the variable ξ can be written as $\xi = \tilde{\xi} + \xi''$ leading to a modified filter $\tilde{\bar{\xi}} = \overline{\rho\xi}/\bar{\rho}$. The filtered equations of the mass, the momentum and the energy are:

$$\partial_t \bar{\rho} + (\bar{\rho}\tilde{u}_j)_{,j} = 0 \tag{1}$$

$$\partial_t (\bar{\rho}\,\tilde{u}_i) + (\bar{\rho}\,\widetilde{\tilde{u}_i\,\tilde{u}_j})_{,j} = (\bar{\sigma}_{ij} - \bar{\rho}\,\widetilde{u_i'' u_j''})_{,j} \tag{2}$$

$$\partial_t(\bar{\rho}\,\tilde{E}) + (\bar{\rho}\,\widetilde{\tilde{E}\,\tilde{u}_j})_{,j} = \left(\overline{\bar{\sigma}_{ij}\tilde{u}_i} - \bar{q}_j\right)_{,j} + \left(\overline{\sigma_{ij}u_i''} - \bar{\rho}\widetilde{E''u_j''}\right)_{,j} \tag{3}$$

where u_i, E, σ_{ij}, q_i are respectively the velocity vector, the total energy, the tensorial term composed of the pressure and the viscous tensor, and the total heat flux vector. In these expressions, the $\bar{\sigma}_{ij}$ tensor takes the form:

$$\bar{\sigma}_{ij} = \bar{\mu}\,(\tilde{u}_{i,j} + \tilde{u}_{j,i}) - (\bar{p}\delta_{ij} + \frac{2}{3}\bar{\mu}\tilde{u}_{k,k}\delta_{ij}) \tag{4}$$

where μ stands for the dynamical molecular viscosity. The subgrid-scale Reynolds stress tensor for the fluctuating velocities is $(\tau_{ij})_{sgs} = \widetilde{u_i'' u_j''}$. The filtered heat flux is computed using Fourier law $\bar{q}_i = -\bar{\chi}\,\partial\tilde{T}/\partial x_i$ where T is the temperature and χ stands for the thermal conductivity. The fluctuating correlation which appears in the right hand side in the energy equation (3) can be developed as $\overline{\sigma_{ij}u_i''} - \bar{\rho}\widetilde{E''u_j''} \approx \bar{\rho}\tilde{u}_i\widetilde{u_i''u_j''} + \bar{\rho}\widetilde{h''u_j''}$ where h is the enthalpy of the fluid. So that the closure of the mean flow equations is necessary for both $(\tau_{ij})_{sgs}$ and the turbulent heat flux $(F_{hi})_{sgs} = \widetilde{h''u_i''}$.

TRANSPORT EQUATIONS SUBGRID-SCALE MODEL

The subgrid equation modeling

The modeling lies on the analyzis of the turbulent processes in the spectral space for homogeneous turbulence. So, the subgrid scale equation terms are derived by partial integration in spectral space. In a subsequent step, the diffusion terms are also implemented in order to account for non homogeneous fields. In this framework, a cutoff wave number κ_c is introduced in the medium range of eddies while the wave number κ_d is located at the end of the inertial range of the spectrum after the transfer zone. The subgrid-scale energy in the range $[\kappa_c, \kappa_d]$ is denoted $k_{sgs} = (\tau_{mm})_{sgs}/2$. We define the dimensionless wave number $\eta_c = \kappa_c\, k^{3/2}/\epsilon$ using the cutoff wave number κ_c and a macro-turbulent length scale computed by means of k and ϵ where k denotes the total turbulent kinetic energy (resolved part and modeled part) and ϵ is the dissipation rate.

The turbulent transport equation of the subgrid-scale tensor $(\tau_{ij})_{sgs} = \widetilde{u_i'' u_j''}$ is modeled in physical space as:

$$\partial_t\left(\bar{\rho}\,(\tau_{ij})_{sgs}\right) + \left(\bar{\rho}\,\overline{(\tau_{ij})_{sgs}\,\tilde{u}_k}\right)_{,k} = P_{ij} - \bar{\rho}\epsilon_{ij} + \Phi^1_{ij} + \Phi^2_{ij} + \Phi^w_{ij} + J_{ij} \tag{5}$$

where

$$P_{ij} = -\overline{\bar{\rho}(\tau_{ik})_{sgs}\tilde{u}_{j,k}} - \overline{\bar{\rho}(\tau_{jk})_{sgs}\tilde{u}_{i,k}} \tag{6}$$

$$\epsilon_{ij} = \frac{2}{3}\epsilon\delta_{ij} \tag{7}$$

The terms on the right-hand side of equation (5) are identified as the production by the filtered velocity P_{ij}, the turbulent viscous dissipation ϵ_{ij}, the redistribution of the subgrid-scale turbulent kinetic energy among the stress components Φ_{ij}, and the diffusion due to the fluctuating velocities and pressure J_{ij} together with the molecular diffusion. The redistribution terms Φ^1_{ij}, Φ^2_{ij} and Φ^w_{ij} of the pressure-strain subgrid-scale fluctuating correlations must be modeled. In the limit of vanishing η_c , the spectral cutoff goes to zero and the assumptions are chosen in order to recover the usual statistical model of Launder and Shima (1989). In compliance with that condition, we propose the following model hypotheses in the range $[\kappa_c, \kappa_d]$:

$$\Phi^1_{ij} = -c_{sgs_1}\bar{\rho}\frac{\epsilon}{k_{sgs}}\left((\tau_{ij})_{sgs} - \frac{2}{3}k_{sgs}\delta_{ij}\right) \tag{8}$$

$$\Phi^2_{ij} = -c_2\left(P_{ij} - \frac{1}{3}P_{mm}\delta_{ij}\right) \tag{9}$$

Equation (8) characterizes non-linear interactions whereas equation (9) represents the linear contribution of the return to isotropy with respect to the velocity gradients. According to the classical physics of turbulence, the coefficient c_{sgs_1} is expected to increase with the parameter η_c in order to increase the return to isotropy in the range of larger wave numbers. We suggest a simple empirical function:

$$c_{sgs_1} = \frac{1 + \alpha_\eta\,\eta_c^2}{1 + \eta_c^2}c_1 \tag{10}$$

where α_η is a numerical constant. This function satisfies the limiting condition $\lim_{\eta_c \to 0} c_{sgs_1}(\eta_c) = c_1$. The function c_1 depends on the second and third subgrid-scale invariants $A_2 = a_{ij}a_{ji}$, $A_3 = a_{ij}a_{jk}a_{ki}$ and the flatness coefficient parameter $A = 1 - \frac{9}{8}(A_2 - A_3)$ where $a_{ij} = ((\tau_{ij})_{sgs} - \frac{2}{3}k_{sgs}\delta_{ij})/k_{sgs}$. The term Φ^w_{ij} takes into account the wall reflexion effect of the pressure fluctuations and is imbedded in the model for reproducing correctly the logarithmic region of the turbulent boundary layer (Gibson and Launder, 1978). The diffusion process J_{ij} is modeled assuming a tensorial gradient law:

$$J_{ij} = \left(\bar{\mu}(\tau_{ij})_{sgs,k} + c_s\bar{\rho}\frac{k_{sgs}}{\epsilon}(\tau_{kl})_{sgs}(\tau_{ij})_{sgs,l}\right)_{,k} \tag{11}$$

where c_s is a numerical coefficient. In contrast to the two-equation model, it can be mentioned that the production term

P_{ij} is allowed to become negative. In such a case, this implies that energy is transfered from the filtered motions up to the resolved motions, known as backscatter process.

The dissipation rate equation by spectral splitting

This equation is modeled by considering the turbulent processes which develop in a spectral slice (Schiestel, 1986). In a first step, the case of homogeneous anisotropic turbulence is considered. The constant value of the mean velocity gradient is denoted Λ_{ij}. The equation of the energy spectrum balance $E(\kappa)$ is:

$$\partial_t E = -\Lambda_{ij} A_{ij} + T - 2\nu\kappa^2 E \tag{12}$$

The three terms on the right hand side of this equation represent the production caused by the mean velocity gradient, the spectral transfer which results from triad interactions of wave number modes, and the viscous dissipation. The term A_{ij} corresponds to the spherical mean of the spectral tensor of the double velocity correlations in wave vector space. Integration of the basic equation (12) over the wave number range $[\kappa_{j-1}, \kappa_j]$ yields the following equation:

$$\partial_t k_{[\kappa_{j-1},\kappa_j]} = P_{[\kappa_{j-1},\kappa_j]} - F(\kappa_j) + F(\kappa_{j-1}) - \epsilon_{[\kappa_{j-1},\kappa_j]} \tag{13}$$

with the relations

$$k_{[\kappa_{j-1},\kappa_j]} = \int_{\kappa_{j-1}}^{\kappa_j} E(\kappa) d\kappa \tag{14}$$

$$P_{[\kappa_{j-1},\kappa_j]} = -\Lambda_{lm} \int_{\kappa_{j-1}}^{\kappa_j} A_{lm}(\kappa) d\kappa \tag{15}$$

$$F(\kappa_j) = \mathcal{F}(\kappa_j) - E(\kappa_j)\, \partial_t \kappa_j \tag{16}$$

$$\mathcal{F}(\kappa) = \int_{\kappa}^{\infty} T(\kappa') d\kappa' = -\int_{0}^{\kappa} T(\kappa') d\kappa' \tag{17}$$

$$\epsilon_{[\kappa_{j-1},\kappa_j]} = 2\nu \int_{\kappa_{j-1}}^{\kappa_j} \kappa^2 E(\kappa) d\kappa \tag{18}$$

$\mathcal{F}$ represents the spectral energy rate transfered into the wave number range $[\kappa, +\infty]$ by vortex stretching from the wave number range $[0, \kappa]$. Equation (13) can be applied for any wave number range such as $[0, \kappa_c]$, $[\kappa_c, \kappa_d]$ and $[\kappa_d, \infty[$. Taking into account the significant processes, one can obtain the following approximated equations:

$$\partial_t (k - k_{sgs}) = P_{[0,\kappa_c]} - F(\kappa_c) \tag{19}$$

$$\partial_t k_{sgs} = P_{[\kappa_c,\kappa_d]} - F(\kappa_d) + F(\kappa_c) \tag{20}$$

$$0 = F(\kappa_d) - \epsilon_{[\kappa_d,\infty[} \tag{21}$$

where $\epsilon_{[\kappa_d,\infty[} \approx \epsilon$. Equation (21) indicates that the dissipation rate ϵ can indeed be interpreted as a spectral flux. In the present approach, the splitting wave number κ_d is assumed to be related to the cutoff wave number κ_c by the dimensional relation:

$$\kappa_d - \kappa_c = \zeta_{sgs} \frac{\epsilon}{{k_{sgs}}^{3/2}} \tag{22}$$

where ζ_{sgs} is a coefficient which may be depended on the spectrum shape and on the Reynolds number. The numerical coefficient ζ_{sgs} is chosen such that κ_d is sufficiently large to encompass the inertial zone and then equation (21) is verified, the energy density beyond κ_d being negligible. The relation (22) is proposed for adjusting the location of the cutoff wave number to the evolving spectrum. The dissipation rate equation is then obtained by taking the derivative of equation (22) with respect to time using equation (16) written for the wave number κ_j:

$$\frac{\partial \kappa_j}{\partial t} = \frac{\mathcal{F}(\kappa_j) - F(\kappa_j)}{E(\kappa_j)} \tag{23}$$

Taking into account (20) and (21), one can easily obtain:

$$\frac{\partial \epsilon}{\partial t} = c_{sgs\epsilon_1} \frac{\epsilon}{k_{sgs}} \left(P_{[\kappa_c,\kappa_d]} + F(\kappa_c) \right) - c_{sgs\epsilon_2} \frac{\epsilon^2}{k_{sgs}} \tag{24}$$

where $c_{sgs\epsilon_1} = 3/2$. Setting $\kappa_d \gg \kappa_c$, and $E(\kappa_d) \ll E(\kappa_c)$, $c_{sgs\epsilon_2}$ takes the form (Chaouat and Schiestel, 2005):

$$c_{sgs\epsilon_2} = c_{sgs\epsilon_1} - \frac{k_{sgs}}{\kappa_d E(\kappa_d)} \left(\frac{\mathcal{F}(\kappa_d)}{\epsilon} - 1 \right) \tag{25}$$

The cutoff wavenumber κ_c is supposed to be known because the filter width can be freely specified. In the case of full statistical modeling where $\kappa_c = 0$, equation (22) is reduced to the equation:

$$\kappa_d = \zeta_d \frac{\epsilon}{k^{3/2}} \tag{26}$$

where the coefficient ζ_d is a numerical constant chosen such that κ_d is located after the inertial range. By taking the derivative of equation (26) with respect to time, using equation (23), another formulation of the dissipation rate equation is then obtained:

$$\frac{\partial \epsilon}{\partial t} = c_{\epsilon_1} \frac{\epsilon}{k} P_{[0,\infty[} - c_{\epsilon_2} \frac{\epsilon^2}{k} \tag{27}$$

where $c_{\epsilon_1} = 3/2$ and

$$c_{\epsilon_2} = c_{\epsilon_1} - \frac{k}{\kappa_d E(\kappa_d)} \left(\frac{\mathcal{F}(\kappa_d)}{\epsilon} - 1 \right) \tag{28}$$

This is in fact the usual ϵ equation used in statistical closures. Equations (25) and (28) show that the coefficients $c_{sgs\epsilon_2}$ and c_{ϵ_2} are functions of the spectrum shape. Keeping in mind that the dissipation rate ϵ must remain the same regardless the location of the wave number κ_c, comparing equation (24) with equation (27) allows to express the coefficient $c_{sgs\epsilon_2}$ in a more convenient form:

$$c_{sgs\epsilon_2} = c_{\epsilon_1} + \frac{k_{sgs}}{k} \left(c_{\epsilon_2} - c_{\epsilon_1} \right) \tag{29}$$

The function k_{sgs}/k which appears in equation (29) can be calibrated by referring to the Kolmogorov law of the three-dimensional energy spectrum in the inertial wave number range in nearly equilibrium flows:

$$E(\kappa) = C_K \epsilon^{2/3} \kappa^{-5/3} \tag{30}$$

where $C_K \approx 1.50$ is the Kolmogorov constant. The subgrid-scale turbulent kinetic energy is then estimated by integrating the Kolmogorov law in the wave number range $[\kappa_c, +\infty[$:

$$k_{sgs} = \int_{\kappa_c}^{\infty} E(\kappa) d\kappa = \frac{3}{2} C_K \epsilon^{2/3} \kappa_c^{-2/3} \tag{31}$$

Taking into account expression of the dimensionless wave number $\eta_c = \kappa_c k^{3/2}/\epsilon$ and equation (31), the ratio k_{sgs}/k is easily obtained by analytical derivation:

$$\frac{k_{sgs}}{k} = \frac{3 C_K}{2} \eta_c^{-2/3} \tag{32}$$

As a result of interest, equation (32) shows that the function k_{sgs}/k is dependant on the parameter $\eta_c^{-2/3}$. The previous result is only valid in the inertial range. It is extended empirically to the general case, taking care to satisfy the limit when k_{sgs} approaches to k, (i.e. when η_c goes to zero). So, the coefficient $c_{sgs\epsilon_2}$ in equation (29) is modeled taking account of equation (32). The empirical choice is proposed:

$$c_{sgs\epsilon_2} = c_{\epsilon_1} + \frac{c_{\epsilon_2} - c_{\epsilon_1}}{1 + \beta_\eta \, \eta_c^{2/3}} \tag{33}$$

where β_η is a numerical constant which takes the theoretical value $\beta_\eta = 2/3C_K \approx 0.444$ in order to satisfy the correct asymptotic behavior in $\eta_c^{-2/3}$ for high values η_c. In the limit of full statistical modeling, $k_{sgs} \to k$ and the usual RSM model is recovered while in the limit $k_{sgs} \to 0$, the subgrid-scale energy is not maintained due to the fact that $c_{sgs\epsilon_2} \to c_{\epsilon_1}$ and the model behaves like a DNS (but the model become useless!).

For non-homogeneous flows, the convection and diffusion terms are imbedded in equation (24). Then, also taking into account low Reynolds number terms, the modeled equation of the dissipation rate can be written as follows:

$$\partial_t(\bar{\rho}\epsilon) + \left(\overline{\bar{\rho}\epsilon\tilde{u}_j}\right)_{,j} = c_{\epsilon_1}\frac{\epsilon}{k_{sgs}}\frac{P_{mm}}{2} - c_{sgs\epsilon_2}\,\bar{\rho}\frac{\tilde{\epsilon}\epsilon}{k_{sgs}} + J_\epsilon \tag{34}$$

where the diffusion process J_ϵ is modeled assuming a tensorial gradient law:

$$J_\epsilon = \left(\bar{\mu}\epsilon_{,j} + c_\epsilon\bar{\rho}\frac{k_{sgs}}{\epsilon}(\tau_{jm})_{sgs}\epsilon_{,m}\right)_{,j} \tag{35}$$

where c_ϵ is a constant coefficient and $\tilde{\epsilon} = \epsilon - 2\nu[(\sqrt{k_{sgs}})_{,n}]^2$. Intuitively, it is obvious that the usual ϵ equation used in statistical modeling in which the whole spectrum is modeled cannot be used without modification in LES in which just a part of the spectrum is modeled. This modification is made here through a variation of the coefficient $c_{sgs\epsilon_2}$ and so the model is allowed to "read "the size of the mesh in order to model only the appropriate portion of the turbulence field. This is the main feature of the present LES model which is basically different from an URANS approach.

Practical formulation

In a practical formulation for the case of wall bounded flows, the length scale can be computed using the normal distance to the wall $L = Kx_3$ where K is the Von Kármán constant. In that condition, we use the alternative dimensionless wave number $\mathcal{N}_c = \kappa_c L$ instead of the previous wave number $\eta_c = \kappa_c \, k^{3/2}/\epsilon$ and we introduce modified coeffcients $\alpha_\mathcal{N}$, $\beta_\mathcal{N}$ in equations (10) and (33). In that framework, the alternative fonctions of the subgrid-scale turbulence model are written more simply in the following way :

$$c_{sgs_1} = \frac{1 + \alpha_\mathcal{N}\,\mathcal{N}_c^2}{1 + \mathcal{N}_c^2}c_1 \tag{36}$$

and

$$c_{sgs\epsilon_2} = c_{\epsilon_1} + \frac{c_{\epsilon_2} - c_{\epsilon_1}}{1 + \beta_\mathcal{N}\,\mathcal{N}_c^{2/3}} \tag{37}$$

The cutoff wave number κ_c is approximated by the filter width:

$$\kappa_c = \frac{\pi}{(\Delta_1\Delta_2\Delta_3)^{\frac{1}{3}}} \tag{38}$$

The large scale part of the Reynolds stress is given by:

$$(\tau_{ij})_{les} = < \bar{u}_i\bar{u}_j > - < \bar{u}_i >< \bar{u}_j > \tag{39}$$

So that the total Reynolds stress τ_{is} is calculated as the sum of the subgrid and large scale parts $\tau_{ij} = (\tau_{ij})_{sgs} + (\tau_{ij})_{les}$.

LES OF FULLY DEVELOPED TURBULENT CHANNEL FLOW

This flow is chosen as a preliminary test case for the proposed approach. Numerical simulations are performed on coarse and refined meshes requiring $16 \times 32 \times 64$ grids (LES 1) and $32 \times 64 \times 84$ grids (LES 2) with different spacings Δ_i. This choice is motivated by the necessity of checking the grid independence of the solution on the numerical point of view as well as the consistency of the subgrid scale model when the filter width is changed. In the normal direction to the wall, the grid points are distributed in non-uniform spacing with refinement near the wall. The numerical simulation of fully developed turbulent channel flow is compared with data obtained by the direct numerical simulation of Moser et al. (1999) for a Reynolds number $R_\tau = \rho_\tau u_\tau \delta/2\mu = 395$, based on the averaged friction density ρ_τ, the averaged friction velocity u_τ and the channel half width $\delta/2$. Several trial and error tests have been made for selecting appropriate values for the two model coefficients $\alpha_\mathcal{N} = 1.5$ and $\beta_\mathcal{N} = 0.5$. Figure (1) shows the evolutions of the normalized total Reynolds stresses computed as the sum of the subgrid and large scale parts (i=1,2,3) for the two different meshes with comparisons with the DNS data. As observed, a good agreement is observed for both LES simulations although the meshes are not refined.

LES OF CHANNEL FLOW WITH WALL INJECTION

The application to the channel flow with wall mass injection which undergoes the possible development of natural unsteadiness (depending on the channel height) with a transition process from laminar to turbulent regime (Chaouat, 2002) is then considered as shown in Figure (2) for illustrating the potentials of the method. The objective is to simulate the flow which develops in the specific experimental setup VECLA made at ONERA. Values of the length, height and width of the channel are respectively $L_1 = 58.1$ cm, $L_2 = 6$ cm and $\delta = 1.03$ cm. The present LES results are compared to the experimental data of Avalon et al. (1998). The numerical 3d simulation is performed on a mesh composed of $400 \times 44 \times 80$ grid points in the streamwise, spanwise and normal directions to the wall. Figure (3) shows the instantaneous spanwise filtered vorticity $\tilde{\omega}_i = \epsilon_{ijk}\tilde{u}_{k,j}$ in different planes of the channel and provides the detail of the flow structures subjected to mass injection as well as the location of the transition. The flow is then characterized by the presence of roll-up vortex structures of large magnitude of vorticity. Because of the injection, it is found that these structures are inclined in the normal direction to the axial flow as previously observed by Apte and Yang (2003). Figure (4) describes the profiles of the streamwise turbulent intensity $< \tau_{11} >^{1/2}/u_m$, where u_m denotes the bulk velocity, in different cross sections and reveals a fair agreement with the experimental data, (However, the measurements are not reliable near the walls).

Other simulation in the Vecla setup for a different channel height $\delta = 2.06$ cm is performed. Contrary to the previous case, the experiment indicates that the flow is then characterized by a low level of turbulence intensity which enables the development of the vortex shedding near the wall. The flow appears oscillating with an acoustic resonant regime which corresponds to the second longitudinal mode (Avalon et al., 1998). This flow has been previously predicted fairly well using a Reynolds stress model (Chaouat and Schiestel, 2002). The objective of the present LES is to provide qualitative details of the flow structures. The mesh is composed of $600 \times 22 \times 60$ grid points in the streamwise, spanwise and normal directions to the wall. In order to trigger the instabilities, a Gaussian forcing has been applied in the immediate vicinity of the permeable wall. Figure (5) shows the instantaneous vorticity contours in different planes of the channel. The development of the acoustic boundary layer chararacterized by horizontal lines is well visible close to the injected wall, in particular from the head end to the exit section of the channel. Figure (5b) which shows the enlarged view of the instantaneous vorticity near the exit reveals the presence of vortex which develop near the injected wall. The analyzis of the pressure signal close to the head end of the channel indicates indeed that the pressure is locally oscillating contrary to the previous case in which the pressure remains perfectly steady in the upstream location of the transition. The present structures appear quite organized in agreement with visualization tests using Acetone Planar Laser-Induceed Fluorescence (PLIF) (Avalon et al., 2000) but differ appreciably from the chaotic structures observed in figure (3) which are developed in a fully turbulent flow regime. The instantaneous vorticity contours described by figure (5c) are still characterized by the injected noise at the wall and reveal that the turbulence intensity is not as so developed than for the previous case (see figure 3b). That useful comparison between these figures shows that the flow structures in a plane channel may evolve differently according to the physical phenomena encountered.

CONCLUSION

A new partially integrated transport model (PITM) for subgrid-scale stresses and dissipation rate has been proposed for LES of unsteady flows which present non-equilibrium turbulence spectra or LES on coarse grids. The use of transport equations for all the subgrid-scale stress components allows to take into account more precisely the turbulent processes and the concept of turbulent viscosity is no longer necessary. The partial integration in spectral space leads to a formal derivation of the model which continuously complies with the variations on the relative cutoff location attached to filter size and which guaranties compatibility with the two extreme limits that are the full statistical Reynolds stress model and direct numerical simulation. The present model has been successfully calibrated on the well known fully turbulent channel flow. The application to the channel flow with wall injection has been then considered for illustrating the potentials of the method.

REFERENCES

Apte, S. A., and Yang, V., 2003, "A Large-eddy Simulation Study of Transition and Flow Instability in a Porous-Walled Chamber with Mass Injection", *Journal of Fluid Mechanics*, Vol. 477, pp. 215-225.

Avalon, G., Casalis, G., and Griffond, J., 1998, "Flow Instabilities and Acoustic Resonance of Channels with Wall Injection", AIAA paper 3218.

Avalon, G., Ugurtas, B., and Grish, F., 2000, "Numerical Computations and Visualization Tests of the Flows Inside a Cold Gas Simulation" AIAA paper 3387.

Chaouat, B., 2001, "Simulations of Channel Flows with Effects of Spanwise Rotation or Wall Injection Using a Reynolds Stress Model", *Journal of Fluid Engineering, ASME*, Vol. 123, pp. 1-9.

Chaouat, B., 2002 "Numerical Predictions of Channel Flows with Fluid Injection Using Reynolds Stress Model", *Journal of Propulsion and Power*, vol. 18, pp. 295-303.

Chaouat, B., and Schiestel, R., 2002, "Reynolds Stress Transport Modelling for Steady and Unsteady Channel Flows with Wall Injection", *Journal of Turbulence*, Vol. 3, pp. 1-15.

Chaouat, B., and Schiestel, R., 2005, "A New Partially Integrated Transport Model for Subgrid-scale Stresses and Dissipation Rate for Turbulent Developing Flows ", *to appear in Physics of Fluids.*

Deardorff, J. W., 1973, "The Use of Subgrid Transport Equations in a Three-dimensional Model of Atmospheric Turbulence", *Journal of Fluid Engineering, ASME*, Vol. 95, pp. 429-438.

Germano, M., Piomelli, U., Moin, P., and Cabot, W. H., 1992, "A Dynamic Subgrid-scale Eddy-viscosity Model", *Physics of Fluids*, Vol. 3, pp. 1760-1765.

Gibson, M. M., and Launder, B. E., 1978, "Ground Effects on Pressure Fluctuations in the Atmospheric Boundary Layer", *Journal of Fluid Mechanics*, Vol. 86, pp. 491-511.

Hanjalic, K., Hadziabdic, M., Temmerman, M. and Leschziner, M., 2004, "Merging LES and RANS Strategies: Zonal or Seamless Coupling ?", *Direct and Large eddy Simulations n° V*, Ed. by R. Friedrich, B. Geurts and O. Métais, Kluwer Academic.

Launder, B. E., 1989, "Second Moment Closure: Present ... and Future?", *Int. J. Heat Fluid Flow*, Vol. 10, pp. 282-300.

Launder, B. E., and Shima, N., 1989, "Second Moment Closure for the Near Wall Sublayer: Development and Application", *AIAA Journal*, Vol. 27, pp. 1319-1325.

Lesieur, M., and Metais, O., 1996, "New Trends in Large-eddy Simulations of Turbulence", *Ann. Rev Journal of Fluid Mechanics*, Vol. 28, pp. 45-82.

Moser, R., Kim, D., and Mansour, N, 1999, "Direct Numerical Simulation of Turbulent Channel Flow up to $R_\tau = 590$", *Physics of Fluids*, Vol. 11, pp. 943-945.

Schiestel, R., 1986, "Multiple-time Scale Modeling of Turbulent Flows in one Point Closures", *Physics of Fluids*, Vol. 30, pp. 722-731.

Schiestel, R., and Dejoan, A., 2005, "Towards a New Partially Integrated Transport Model for Coarse Grid and Unsteady Turbulent Flow Simulations", *Theoret. Comput. Fluid Dynamics*, Vol. 18, pp. 443-468.

Spalart, P. R., 2000, "Strategies for Turbulence Modelling and Simulations", *International Journal of Heat and Fluid Flow*, Vol. 21, pp. 252-263.

Speziale, C. G., Sarkar, S., and Gatski, T. B., 1991, "Modelling the Pressure-Strain Correlation of Turbulence: an Invariant Dynamical Systems Approach", *Journal of Fluid Mechanics*, Vol. 227, pp. 245-272.

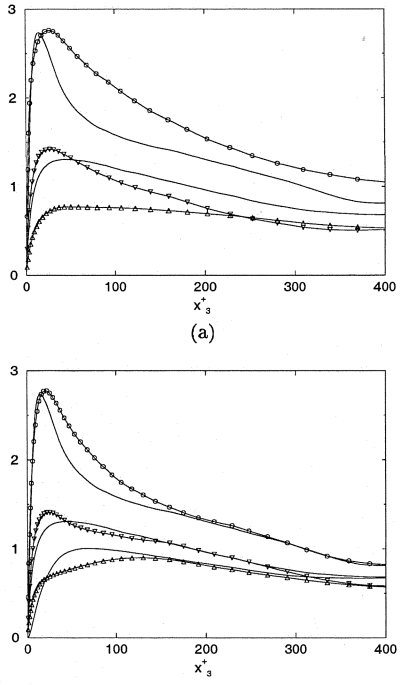

Figure 1: Turbulent Reynolds stresses $(< (\tau_{ii})_{sgs} > + < (\tau_{ii})_{les} >)^{\frac{1}{2}} / u_\tau$. (a) LES 1; (b) LES 2; $\circ : i = 1$, $\Delta: i = 2$, $\nabla : i = 3$; —: DNS.

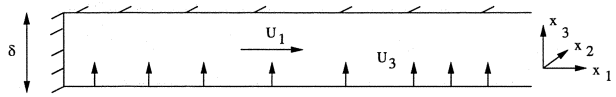

Figure 2: Schematic of channel flow with fluid injection.

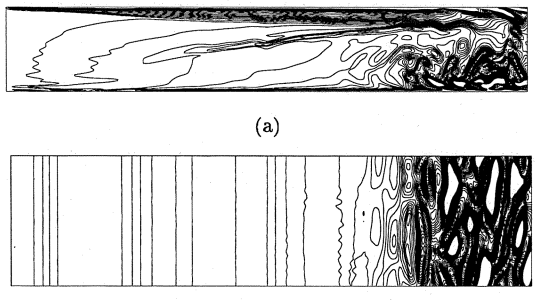

Figure 3: Snapshots of spanwise instantaneous filtered vorticity, $\delta = 1.03$ cm. $-4.10^4\, s^{-1} < \tilde{\omega} < 4.10^4 s^{-1}$, $\Delta\omega = 2000$ s^{-1}. (a) plane (x_1, x_3), $x_2/\delta = 1$; (b) plane (x_1, x_2), $x_3/\delta \approx 0$.

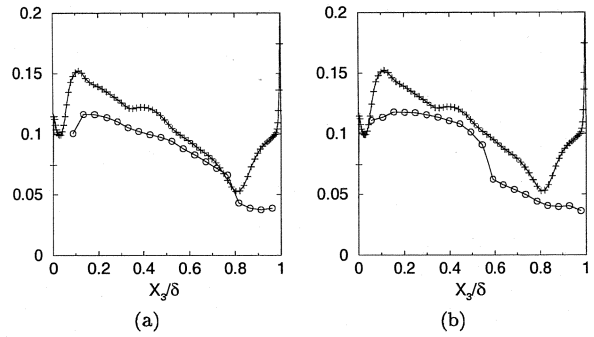

Figure 4: Streamwise turbulent stresses. +: $< (\tau_{11})^{\frac{1}{2}} > / u_m$; $\circ$: experimental data; (a) 50 cm; (b) 57 cm.

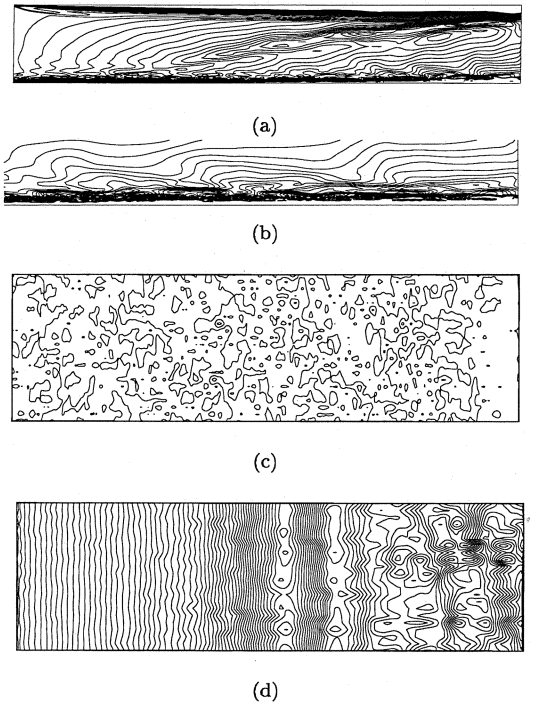

Figure 5: Snapshots of spanwise instantaneous filtered vorticity, $\delta = 2.06$ cm. $-4.10^3\, s^{-1} < \tilde{\omega} < 6.10^3 s^{-1}$. (a) plane (x_1, x_3), $x_2/\delta = 1$, $\Delta\omega = 200$ s^{-1}; (b) Enlarged view in the lower wall region near the exit. plane (x_1, x_3), $x_2/\delta = 1$, $\Delta\omega = 200$ s^{-1}; (c) plane (x_1, x_2), $x_3/\delta \approx 0$, $\Delta\omega = 1000$ s^{-1}; (d) plane (x_1, x_2), $x_3/\delta = 0.5$, $\Delta\omega = 50$ s^{-1}.